Micromechanics Modeling of Functionally Graded Interphase Regions in Carbon Nanotube-Polymer Composites

Gary D. Seidel* and Dimitris C. Lagoudas †
Texas A&M University, College Station, TX, 77843-3141, USA
Sarah Jane V. Frankland‡
National Institute of Aerospace, Hampton, VA, 23666-1399, USA
Thomas S. Gates§
NASA Langley Research Center, Hampton, VA, 23681, USA

The effective elastic properties of a unidirectional carbon fiber/epoxy lamina in which the carbon fibers are coated with single-walled carbon nanotubes are modeled herein through the use of a multi-scale method involving the molecular dynamics/equivalent continuum and micromechanics methods. The specific lamina representative volume element studied consists of a carbon fiber surrounded by a region of epoxy containing a radially varying concentration of carbon nanotubes which is then embedded in the pure epoxy matrix. The variable concentration of carbon nanotubes surrounding the carbon fiber results in a functionally graded interphase region as the properties of the interphase region vary according to the carbon nanotube volume fraction. Molecular dynamics and equivalent continuum methods are used to assess the local effective properties of the carbon nanotube/epoxy comprising the interphase region. Micromechanics in the form of the Mori-Tanaka method are then applied to obtain the global effective properties of the graded interphase region wherein the carbon nanotubes are randomly oriented. Finally, the multi-layer composite cylinders micromechanics approach is used to obtain the effective lamina properties from the lamina representative volume element. It was found that even very small quantities of carbon nanotubes (0.36% of lamina by volume) coating the surface of the carbon fibers in the lamina can have a significant effect (8% increase) on the transverse properties of the lamina (E_{22}, κ_{23}, G_{23} and G_{12}) with almost no affect on the lamina properties in the fiber direction (E_{11} and ν_{12}).

Nomenclature

$\mathbf{A}^{\text{glob}}$ Strain concentration factor tensor in global coordinate system
$\mathbf{A}^{\text{loc}}$ Strain concentration factor tensor in local coordinate system
$\tilde{\mathbf{A}}^{\text{loc}}$ Dilute strain concentration factor tensor in local coordinate system
$B_i^{(j)}$ Displacement field constant of the j^{th} layer
$\mathbf{C}$ Effective stiffness tensor in global coordinate system
c_f Fiber volume fraction
$\mathbf{C}_f^{\text{glob}}$ Fiber stiffness tensor in global coordinate system, Pa
$\mathbf{C}_f^{\text{loc}}$ Fiber stiffness tensor in local coordinate system, Pa
$\mathbf{C}_m$ Matrix stiffness tensor, Pa

*Graduate Student, Aerospace Engineering Department, AIAA Student Member.
†Professor, Aerospace Engineering Department, AIAA Member.
‡Senior Research Scientist, AIAA Member.
§Senior Materials Research Engineer, Mechanics of Structures and Materials Branch, AIAA Associate Fellow.

C_{11} Axial stiffness component for transversely isotropic material, Pa
E_{11} Axial Young's modulus for transversely isotropic material, Pa
E_{22} Transverse Young's modulus for transversely isotropic material, Pa
$\mathbf{I}$ Fourth order identity tensor
N Total number of layers in the composite cylinder assemblage, m
L Length of composite cylinder assemblage
r Radial position in cylindrical coordinates
r_j Radial layer boundary, m
$\mathbf{S}^{\text{loc}}$ Eshelby tensor in local coordinate system
$u_r^{(j)}$ Radial displacement component of the j^{th} layer, m
$u_z^{(j)}$ z-direction displacement component of the j^{th} layer, m
$u_\theta^{(j)}$ θ-direction displacement component of the j^{th} layer, m
V Volume, m^3
V_o Volume fraction of carbon nanotubes in Region II
v_0 Initial volume fraction of carbon nanotubes in Region III
W Volume averaged strain energy of the composite cylinder assemblage, N/m^4
$W^{(\text{eff})}$ Volume averaged strain energy of the effective material, N/m^4
X_i Global coordinate direction
x_i Local coordinate direction
Δ Thickness of Region III, m
ε_0 Applied strain
$\varepsilon_{ij}^{(k)}$ Small strain components of the j^{th} layer
κ_{23} Plane strain bulk modulus for transversely isotropic material, Pa
λ_i Lame constant for isotropic phase, Pa
μ_i Lame shear constant for isotropic phase, Pa
μ_{12} Axial shear modulus for transversely isotropic material, Pa
μ_{23} Transverse shear modulus for transversely isotropic material, Pa
ν_{12} Axial Poisson's ratio for transversely isotropic material
$\sigma_{ij}^{(k)}$ Cauchy stress components of the j^{th} layer, Pa

Subscripts and Superscripts
i Variable number
j Variable number
(j) Variable layer designation in composite cylinders model
k Variable number
r Radial component in cylindrical coordinates
z z-direction component in cylindrical coordinates
θ θ-direction component in cylindrical coordinates

I. Introduction

APPLICATIONS for carbon nanotubes (CNTs) in aerospace vehicles are likely to focus in the near term on the enhancement of the mechanical, thermal and electrical properties of materials currently in use. The exceptional properties of CNTs and their relatively low density are believed to be able to provide large improvements in properties with only small quantities of CNTs. For example, enhancements in elastic Young's modulus of unfunctionalized CNTs in CNT-epoxy composites of up 20% in tension and 75% in compression have been observed for CNT volume fractions of just 5%.[1] For functionalized CNTs, that is CNTs which have been chemically altered to better interact with a given matrix, increases in Young's modulus of 30% and 60% have been observed at volume fractions of 1 and 4%, respectively.[2,3] As such, one proposed implementation of CNTs is as structural enhancement of traditional carbon fiber/epoxy composite laminates, as shown schematically in Figure 1, where it is believed that the selective use of CNTs as surface treatments can improve interface strength between the carbon fibers and epoxy, and thereby improve the fracture toughness of the composite.

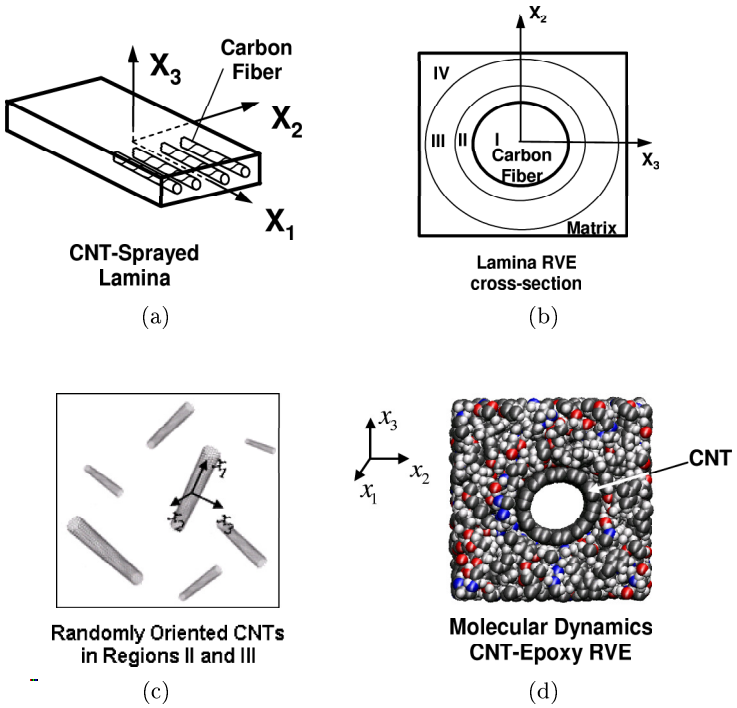

Figure 1. Motivation: CNT-Sprayed Carbon Fiber Composite Analysis Scales (a) Lamina Scale (mm); (b) Lamina RVE Scale (μm); (c) Region II and III Scale (μm^{-1}); (d) CNT RVE Scale (nm)

As a result of the inclusion of nanoscale materials, analysis of such composites, often termed nanocomposites, requires the development of multi-scale models which can span the inherent nanometer to millimeter and beyond length scales. For example, in the composite laminate schematic of Figure 1, the carbon fiber lamina has dimensions on the order of millimeters, the lamina representative volume element (RVE) (Figure 1(b) is on the order of microns, the CNT coating surrounding a carbon fiber (Figure 1(c)) on the order of a tenth of a micron, and finally the CNT RVE in Figure 1(d) is on the order of nanometers. Modeling across such disparate length scales necessitates the use of tools such as molecular dynamics (MD), micromechanics, composite laminate analysis, and finite element modeling.

Multi-scale models have been applied using both atomistic simulations and micromechanics to assess the constitutive properties of various functionalized nanotube materials.[4–9] Other researchers have used atomistic simulations of epoxy/nanotube composites in order to address nanotube pull-out from the epoxy.[10] A more recent study on nanotubes chemically bonded into the epoxy matrix showed a Young's modulus of up to 160 GPa in the direction of the nanotube axis, and 4-8 GPa in the transverse direction at a nanotube volume fraction of 25%.[11]

In the present work, the constitutive properties of a unidirectional carbon fiber/epoxy lamina in which each carbon fiber is coated with CNTs are investigated. The large difference in scales between the carbon fiber, with radius on the order of microns, and the carbon nanotubes, with radius on the order of nanometers, suggests the use of a multi-scale approach. The multi-scale approach herein makes use of molecular dynamics simulations and the equivalent continuum method on the CNT scale and continuum micromechanics analysis on the carbon fiber interphase and lamina scales in assessing effective lamina elastic properties. The objective is to calculate the effective elastic constants of unidirectionally-reinforced carbon fiber/epoxy laminae, where the CNT distribution around the fiber is varied from a high concentration near the carbon fiber surface to zero CNT concentration as a result of the spraying the process. The constitutive properties of the nanoscale components are modeled with the molecular dynamics-equivalent continuum model. The CNT orientation and distribution in volume fraction are modeled using the results of the molecular dynamics-equivalent continuum model in a Mori-Tanaka micromechanics approach to calculate the effective properties of randomly oriented CNTs in epoxy. Finally, the multi-layer composite cylinders method is applied to the lamina representative volume element to obtain the effective lamina properties for carbon fibers in epoxy

surrounded by a graded interphase of varying CNT concentration. A description of each stage of the multi-scale model is presented, and the results of applying the multi-scale approach are given for several types of CNT coatings in the lamina.

II. Micromechanics Modeling

A. Multi-layer Composite Cylinders Model

The composite cylinders method was originally proposed by Hashin and Rosen[12] to obtain the effective elastic constants of unidirectional fiber reinforced composites. In this method, a set of five elasticity solutions are obtained for both a composite cylinder assemblage (cylindrical fiber surrounded by cylindrical matrix) and for a transversely isotropic effective homogeneous cylinder. The strain energy of the composite cylinder assemblage is equated to that of the effective cylinder, and the five independent effective elastic constants are determined. The composite cylinders method of Hashin and Rosen worked well for four of the five independent elastic constants of the effective transversely isotropic material, but could only provide bounds on the fifth, the effective transverse shear modulus (μ_{23}).

Christensen and Lo[13] proposed an alternate model for the effective transverse shear modulus in the form of the generalized self-consistent composite cylinder in which the original composite cylinder assemblage is surrounded by an additional concentric cylinder having the same elastic properties as the effective homogeneous cylinder. The generalized self-consistent composite cylinder solution resulted in an explicit solution for the effective transverse shear modulus that fit within the Hashin and Rosen bounds. The methods of Hashin and Rosen and Christensen and Lo were later consolidated and and generalized in applications involving coated fiber composites[14,15] resulting in a multi-layer composite cylinders method (Figure 2). Recently,[16] multi-layer composite cylinders models have been applied to carbon nanotube reinforced epoxies wherein carbon nanotubes have been treated as continuum sheets of rolled graphene surrounded by interphase layers to simulate differing amounts of load transfer as a result of functionalization, but have lacked direct MD coupling.

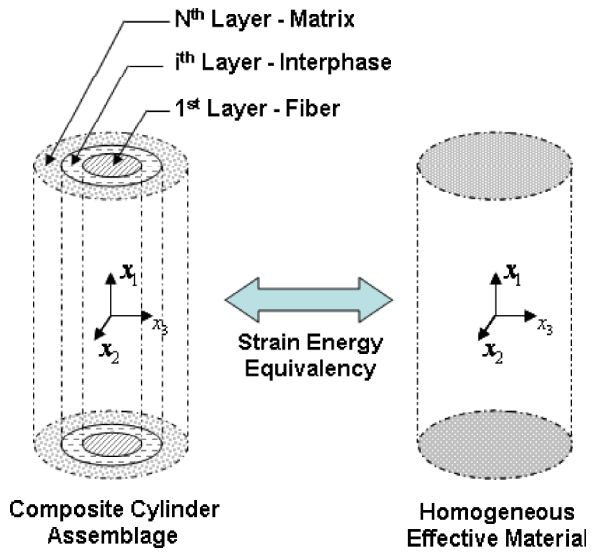

Figure 2. Schematic representation of the composite cylinder method. The composite cylinder assemblage (left) consists of N concentric cylinders whose strain energy under load is equivalent to that of an effective homogeneous material (right).

In the present work, the effective properties for the carbon fiber lamina RVE are obtained using the multi-layer composite cylinder. As shown in Figure 1(b), the layers are the carbon fiber (Region I), the high concentration of carbon nanotubes interphase region (Region II), the variable concentration of carbon nanotubes interphase region (Region III), and the epoxy matrix (Region IV). As an example, the procedure for determining the effective plane strain bulk modulus (κ_{23}) for the lamina RVE is provided. Each layer of the composite cylinder assemblage is taken to have the following displacement field (in cylindrical coordinates with $x_1 = z$):

$$\begin{aligned} u_r^{(j)} &= B_1^{(j)} r + B_2^{(j)} \frac{1}{r} \\ u_\theta^{(j)} &= 0 \qquad\qquad \text{for } r_{j-1} \le r \le r_j \\ u_z^{(j)} &= 0 \end{aligned} \tag{1}$$

where the superscript (j) denotes the region (either I, II, III or IV) and $B_1^{(j)}$ and $B_2^{(j)}$ are constants. The range of each layer is defined by the inner and outer radii, r_{j-1} and r_j, respectively, with $r_0 = 0$ for Region I and r_N for Region IV dependent on the carbon fiber volume fraction. The strains in each layer

are determined from the displacement fields using the small strain strain-displacement relations, with the layer stresses determined from the appropriate constitutive relation for each layer (isotropic linear elastic for Regions I-IV). The constants $B_1^{(j)}$ and $B_2^{(j)}$ are determined through the application of boundary conditions and interface matching conditions. The boundary conditions for determining the plane strain bulk modulus are given by:

$$u_r^{(N)}|_{r=r_N} = \varepsilon_0 r_N \tag{2}$$

$$B_2^{(1)} = 0 \tag{3}$$

where ε_0 is the radial strain applied at the boundary and Eqn. (3) insures that the displacement in Region I is bounded at r_0. The matching conditions at the layer interfaces impose the continuity of displacement and traction conditions and are again given by:

$$u_r^{(k)}|_{r=r_k} = u_r^{(k+1)}|_{r=r_k} \tag{4}$$

$$\sigma_{rr}^{(k)}|_{r=r_k} = \sigma_{rr}^{(k+1)}|_{r=r_k} \tag{5}$$

where k ranges from one to $N-1$. Thus, we have a system of $2N$ equations to solve for the $2N$ unknown constants in the displace field, $B_i^{(j)}$.

The elasticity solution for the effective homogeneous cylinder follows the same procedure. The displacement field in the homogeneous cylinder is taken to be given by:

$$\begin{aligned} u_r^{(\text{eff})} &= B_1^{(\text{eff})} r + B_2^{(\text{eff})} \frac{1}{r} \\ u_\theta^{(\text{eff})} &= 0 \qquad\qquad \text{for } 0 \le r \le r_N \\ u_z^{(\text{eff})} &= 0 \end{aligned} \tag{6}$$

where the superscript (eff) denotes the effective homogeneous material. Again the strains are determined from the strain-displacement relations and the stresses from the constitutive relations which, for the effective homogeneous cylinder, are the unknown effective constants of a transversely isotropic material. The boundary conditions are the same as those applied in Eqns. (2) and (3), and no matching conditions are necessary as the material is homogeneous.

Having solved for all of the unknown constants in the displacement field, the volume averaged strain energies of the composite cylinder assemblage, W, and of the effective homogeneous cylinder, $W^{(\text{eff})}$, can be obtained from:

$$W = \langle \sigma_{ij} \varepsilon_{ij} \rangle \tag{7}$$

and

$$W^{(\text{eff})} = \langle \sigma_{ij}^{(\text{eff})} \varepsilon_{ij}^{(\text{eff})} \rangle \tag{8}$$

where in both equations the summation convention is invoked, and where the lack of superscripts in Eqn. (7) is intended to indicate that the stress and the strain in the brackets is for the composite cylinder assemblage as a whole, i.e, across all layers. The brackets denote the volume average as follows:

$$\langle \bullet \rangle = \frac{1}{V} \int_V \bullet \, dV \tag{9}$$

It can be shown that volume averaged strain energy of the effective homogeneous cylinder can be expressed as:

$$W^{(\text{eff})} = 4\kappa_{23} \varepsilon_0^2 \tag{10}$$

The volume averaged strain energy of the composite cylinder assemblage can be expressed in terms of the stress and strain in the layers as:

$$W = \frac{1}{V} \left(\sum_{(k)=1}^{N} \int_{-L/2}^{L/2} \int_{r_{k-1}}^{r_k} \int_0^{2\pi} \sigma_{ij}^{(k)} \varepsilon_{ij}^{(k)} r \, d\theta \, dr \, dz \right) \tag{11}$$

The effective plane strain bulk modulus is then determined from equating the volume averaged strain energies of the composite cylinder assemblage and the effective homogeneous cylinder, i.e.:

$$W = W^{\text{eff}} \tag{12}$$

It can be shown that Eqn. (12) can be solved for κ_{23} which can be expressed in the following form which depends only on the stress and displacement of the N^{th} phase:

$$\kappa_{23} = \frac{\sigma_{rr}^{(N)}|_{r=r_N}}{2\left(u_r^{(N)}|_{r=r_N}/r_N\right)} \tag{13}$$

which is analogous to the definition of the plane strain bulk modulus given by $\kappa_{23} = \sigma_{22}/2\varepsilon_{22}$. Eqn. (13) can then be expressed in terms of the now known constants $B_i^{(N)}$ as:

$$\kappa_{23} = \frac{(\mu_N + \lambda_N) r_N^2 B_1^{(N)} - \mu_N B_2^{(N)}}{r_N^2 B_1^{(N)} + B_2^{(N)}} \tag{14}$$

where it is has been assumed that the N^{th} phase is isotropic (μ_N and λ_N are the Lamé constants of the N^{th} phase, i.e., Region IV). Similar procedures are followed for obtaining the remaining four transverse isotropy constants: the axial Young's modulus, E_{11}, the axial stiffness component, C_{11}, the axial shear modulus, μ_{12}, and the transverse shear modulus, μ_{23}.[15,16] From these five, other properties such as the transverse Young's modulus, E_{22}, and the axial Poisson's ratio, ν_{12} can be calculated.

B. Effective Properties of Randomly Oriented Fibers

In order to identify constitutive properties for Regions II and III of the lamina RVE in Figure 1(b), it is necessary to consider the effective properties of randomly oriented CNTs. Current MD simulations would find it computationally difficult to model an RVE of sufficient size to consider all possible orientations of CNTs needed to capture the effects of random orientation. As such, micromechanics tools in the form of the Mori-Tanaka method[17,18] are employed in a randomization procedure.

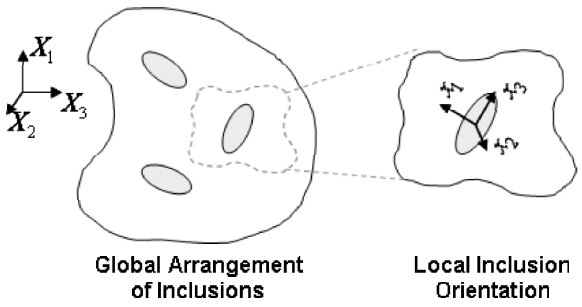

Figure 3. Schematic representation of the randomization procedure. Each inclusion's stiffness and concentration factor in the local coordinate system (x_i) are rotated to the global coordinate system (X_i) and averaged as a separate phase.

The randomization procedure is shown schematically in Figure 3. Inclusions, in this case CNTs, at each distinct orientation relative to the global coordinate system (X_i) of the composite are considered as separate phases in a multi-phase Mori-Tanaka approach. However, in the local inclusion coordinate system (x_i), the inclusions are identical and therefore have the same strain concentration factor in the local coordinate system given by:

$$\mathbf{A}^{\text{loc}} = \tilde{\mathbf{A}}^{\text{loc}} \left[(1 - c_f)\mathbf{I} + c_f \tilde{\mathbf{A}}^{\text{loc}}\right]^{-1} \tag{15}$$

where $\tilde{\mathbf{A}}^{\text{loc}}$ is the Mori-Tanaka dilute strain concentration factor which can be expressed as:

$$\tilde{\mathbf{A}}^{\text{loc}} = \left[\mathbf{I} + \mathbf{S}^{\text{loc}}(\mathbf{C}_m)^{-1}(\mathbf{C}_f^{\text{loc}} - \mathbf{C}_m)\right]^{-1} \tag{16}$$

where c_f is the phase volume fraction, $\mathbf{I}$ is the fourth order identity tensor, $\mathbf{S}$ is the Eshelby tensor[19] (in this case for a circular cylinder), and $\mathbf{C}_m$ and $\mathbf{C}_f$ are the matrix and fiber stiffness tensors, respectively. The superscript loc in Eqns. (15) and (16) indicates that the given quantity is expressed in the local coordinate system, and it is noted that the matrix is assumed to be isotropic so that the local and global coordinate representations of the matrix stiffness ($\mathbf{C}_m$) are the same.

The orientation of the local coordinate system of a given phase relative to the global coordinate system of the composite is expressed in terms of general Euler angle rotations. Subsequently, a general change of basis is applied to rotate the local stiffness tensor and concentration factor into their global coordinate system representations, $\mathbf{C}_f^{\text{glob}}$ and $\mathbf{A}^{\text{glob}}$, respectively. The effective properties for the composite in the global coordinate system can then be expressed as:

$$\mathbf{C} = \mathbf{C}_m + c_f(\mathbf{C}_f^{\text{glob}} - \mathbf{C}_m)\mathbf{A}^{\text{glob}} \tag{17}$$

Finally, the effective properties of the composite as a whole are then obtained by integrating the second term of Equation 17 over all orientations, and are found to isotropic.

III. Application: CNT-sprayed Carbon Fiber Lamina

The multi-layered composite cylinder method and the micromechanical randomization procedures described above are applied in the modeling of CNT-sprayed unidirectional carbon fiber-epoxy composites (Figure 1). The lamina, Figure 1(a), is constructed such that the carbon fibers are first coated with CNTs, and then cured in epoxy. The schematic in Figure 1(a) also identifies the principal material axes with respect to the fiber direction, with X_1 referred to as the longitudinal, or axial direction, and X_2 and X_3 referred to as the transverse, or in-plane directions. The epoxy of interest is comprised of bisphenol F resin reacted with epichlorohydrin and cured with triethylenetetramine (TETA). The CNTs sprayed on the carbon fiber were taken as (10,10) single-walled carbon nanotubes with a radius 0.678 nm. As the CNTs are not functionalized, nor are they grown on the carbon fiber surface, it is assumed in the model that there is no chemical bonding between the 3 components: carbon fiber, carbon nanotubes, and the epoxy.

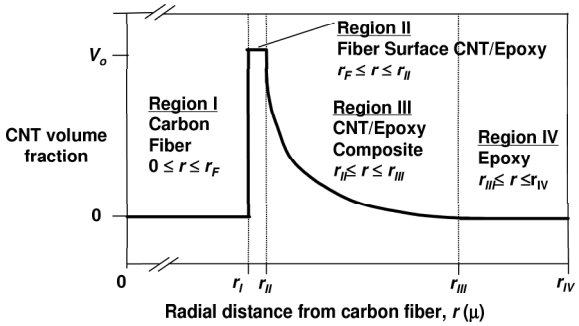

Figure 4. Distribution of CNT volume fraction around the carbon fiber for the Lamina RVE in Figure 1(b). Region II represents a region of higher CNT volume fraction near the carbon fiber surface. Region III represents a larger region of decaying CNT volume fraction which decays according to Eq. (18).

The effective properties of the lamina in Figure 1(a) are determined through the application of the multi-layer composite cylinders method on the lamina RVE shown in Figure 1(b) (X_1-axis, positive out-of-the-page). The RVE identifies four regions. Region I is the carbon fiber itself, where r_{F} represents the carbon fiber radius (taken as $5\,\mu m$). Region II represents a region of relatively high CNT volume fraction very near the carbon fiber surface, and ranges from the carbon fiber radius at r_{F} to r_{II} for a thickness of 0.004 microns. Region III represents a much larger CNT rich region surrounding the carbon fiber where the CNT volume fraction decays from a value close to that of Region II to a zero volume fraction of CNTs. Both Region II and III are comprised of randomly oriented CNTs and epoxy (Figure 1(c)). The width of Region III ranges from r_{II} to r_{III}, and is denoted by the parameter Δ, where $\Delta = r_{\text{III}} - r_{\text{II}}$ and takes a value of $0.3\,\mu m$. Region IV is the remaining epoxy matrix (i.e., no CNTs), and ranges from r_{III} to a maximum radius denoted by the parameter r_{IV} which is determined based on the *carbon fiber* volume fraction.

A detailed graphical representation of the CNT volume fraction distribution versus radial distance from the carbon fiber center for each region of the lamina RVE is shown in Figure 4. Regions I and IV, the carbon fiber and the epoxy matrix, respectively, contain no CNTs and thus have a CNT volume fraction of zero. The CNT volume fraction in Region II is constant and is defined by the parameter V_o, shown in Figure 4, which is taken to be 15.55%. The CNT volume fraction in Region III decays from a value v_0 to zero as the radial distance from the carbon fiber increases. The method of decay for the CNT volume fraction in Region III is given by Eqn. (18):

$$v_f(r) = v_0 \mathrm{e}^{-\alpha(r-r_{II})} - \left(\frac{r - r_{II}}{\Delta}\right) v_0 \mathrm{e}^{-\alpha\Delta} \tag{18}$$

where $\alpha = 9$, $v_0 = 0.1535$, and $\Delta = 0.3\,\mu m$ is radial thickness of Region III. It should be noted that the thicknesses and distribution of CNT volume fractions in Regions II and III are assumed values for modeling

purposes as at present there is insufficient characterization of the fabricated composites to determine these values experimentally.

With the microstructure of the lamina RVE identified, the procedure for determining the effective lamina properties is outlined as follows. First, MD simulations are used to generate representative volume elements of the of the CNT-epoxy constituents of Regions II and III (Figure 1(d)). Second, the equivalent-continuum model[20] is used in conjunction with these MD simulations to calculate the continuum level elastic constants of the CNT-epoxy RVEs. Next, the elastic constants of randomly oriented CNTs in epoxy are calculated as a function of CNT volume fraction using the Mori-Tanaka method. The elastic constants determined from Mori-Tanaka randomization are then mapped onto the CNT volume fraction distribution of Figure 4 to obtain the distribution of elastic constants as a function of radial distance from the carbon fiber for Regions II and III. Finally, the multi-layer composite cylinders method is applied to the lamina RVE using the mapped distribution in elastic constants. These steps are discussed in detail below, as are results obtained from the applying them towards determining the effective properties of the CNT-sprayed carbon fiber composite lamina described above.

A. Molecular Dynamics-Equivalent Continuum CNT-Epoxy Modeling

Molecular dynamics simulations of CNTs in epoxy are performed for the molecular RVE shown in Figure 1(d). The RVE of the molecular structure of the material system was generated via initial energy minimization in the MD simulations and is reflective of a CNT volume fraction of approximately 15%. The molecular structure of the epoxy was a network of bisphenol F resin molecules reacted with epichlorohydrin and cross-linked via triethylenetetramine (TETA) molecules. The TETA molecule is able to cross-link with up to four resin chains, and on average 2.3 of the 4 TETA amine groups in the resultant structure were involved in cross-linking. The equilibrium structure of the CNT-epoxy RVE was obtained by compressing the epoxy network until the minimum potential energy configuration at finite temperature (300 K) was reached.

Table 1. The elastic constants (GPa) obtained from the MD-equivalent continuum method and the corresponding engineering constants (GPa, except ν_{12}) obtained from Eqns. (19) through (24).

MD-Equivalent Continuum				**Graphite CNT**
Elastic Constants		**Engineering Constants**		
C_{11}	99.00	E_{11}	93.44	109.30
C_{22}	12.20	E_{22}	0.40	2.28
C_{12}	8.20	ν_{12}	0.34	0.37
C_{23}	12.00	κ_{23}	12.10	3.83
C_{44}	0.20	G_{23}	0.10	0.67
C_{66}	0.33	G_{12}	0.16	0.69

The CNT-epoxy RVE was simulated with the AMBER force field[21] using the LAMMPS[22] and DL-POLY[23] simulation codes. All of the CNT and graphite parameters were taken from the AMBER force field. Several of the force field parameters of the epoxy network were derived from ab initio calculations carried out with the NWChem package.[24] The partial atomic charges were derived from an RESP fit to a Hartree-Fock calculation of wavefunction. The bond lengths, angles, and dihedrals, were calculated by optimizing the geometry of parts of the epoxy network at the HF/STO-3G level. Partial charges were then fit at this geometry from a HF/6-31G* calculation. The rest of the parameters, were taken from the AMBER force field. In the simulations, electrostatic interactions were calculated with Coulomb's law, and an Ewald summation was used for the long range Coulombic interactions. Electrostatic interactions and 1-4 non-bonded dihedral interactions were scaled by the standard AMBER parameters of 0.83 and 0.50 respectively.

In the MD simulations the molecular structure RVE is subjected to periodic boundary conditions in all three directions. The displacement fields from Ref.,[7] which are consistent with those used in obtaining continuum level elastic properties, were applied to the RVE structure in strain increments of 0.0025 every 10,000 steps at 1 fs each (10 ps per increment) up to a maximum strain of greater than 0.02. The application of the displacement field included displacing both the periodic boundaries and the atomic positions, then equilibrating the system with MD to its new state point. The elastic constants were then obtained for the molecular RVE from equating the energies of deformation for the molecular system, which were calculated from molecular dynamics simulation, to the energies of deformation of an equivalent continuum homogeneous

solid under identical deformations.

The effective stiffness tensor components for the CNT-epoxy system obtained using the MD/equivalent continuum methods are provided in Table 1. Also provided in Table 1 are the expression of the stiffness tensor in terms of the engineering elastic constants for transversely isotropic materials, with the relationships between the two representations given in Eqns. (19) through (24).

$$E_{11} = C_{11} - \frac{C_{12}^2}{C_{22} + C_{23}} \tag{19}$$

$$E_{22} = C_{22} + \frac{C_{12}^2(2C_{23} - C_{22}) - C_{23}^2 C_{11}}{C_{11}C_{22} - C_{12}^2} \tag{20}$$

$$\nu_{12} = \frac{C_{12}}{C_{22} + C_{23}} \tag{21}$$

$$\kappa_{23} = \frac{1}{2}(C_{22} + C_{23}) \tag{22}$$

$$G_{23} = \frac{1}{2}(C_{22} - C_{23}) \tag{23}$$

$$G_{12} = \frac{1}{2}C_{66} \tag{24}$$

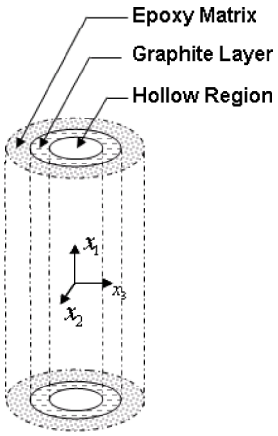

Figure 5. Composite cylinder assemblage used in initial micromechanics evaluation of the effective properties of CNT-epoxy composites.[16] The resulting effective properties of this composite cylinder assemblage are compared with those obtained from MD-equivalent continuum correspondence of the MD-RVE in Figure 1(d) in Table 1.

For comparison purposes, the effective properties of CNTs embedded in epoxy at 15% volume fraction obtained using the composite cylinders solution are also provided in Table 1.[16] In these solutions, the composite cylinder assemblage consists of a hollow and solid portion of the CNT surrounded by the epoxy matrix as shown in Figure 5. Here the composite cylinder method describe above is applied for $N = 2$, with the hollow region accounted for through the application of traction free conditions on the CNT inner surface. As such, the only difference for the composite cylinders method is the change of the boundary condition in Eqn. (3) to $\sigma_{rr}^1|_{r=r_0} = 0$, with r_0 equal to the CNT inner radius of $0.54nm$. The CNTs are thus represented as a rolled sheet of graphene, with the solid portion of the CNT having isotropic properties reflective of the in-plane properties of graphene ($E = 1100GPa$, $\nu = 0.14$).[25] Table 1 indicates that the composite cylinders evaluation of the effective CNT-epoxy properties differs greatly from the MD-equivalent continuum values, especially for E_{22}, κ_{23}, G_{12} and G_{23}. It is of interest to note that these four properties have been observed to be largely affected by the presence of interphase regions.[16] The MD simulations used to obtain the effective CNT-epoxy properties would automatically and accurately include the presence of an interphase region, which is believed to be the source of the large differences observed in Table 1.

B. Random Orientation of Effective CNT-Epoxy Properties

The CNTs in Regions II and III are assumed to be randomly oriented. As such, the effective CNT-epoxy properties from the MD-equivalent continuum method provided in Table 1 are used to define the local stiffness and Eshelby tensor of Eqn. (16). Here the Eshelby tensor applied is for a circular cylinder in an isotropic matrix as the surrounding epoxy is considered to be isotropic linear elastic. The global averaging procedure of Eqn. (17) was applied to obtain the stiffness tensor for the randomly oriented CNT-epoxy system in Regions II and III. Despite being locally transversely isotropic, the effective properties obtained from the global averaging process are isotropic. As such, the effective Young's modulus (E) and Poisson's ratio (ν) for Regions II and III as a function of CNT volume fraction are obtained and provided in Figures 6(a) and 6(b), respectively. The Young's modulus and Poisson's ratio versus CNT volume fraction are

then mapped into the CNT volume fraction distribution of Figure 4 so that the material properties and material property variation of Regions II and III are identified.

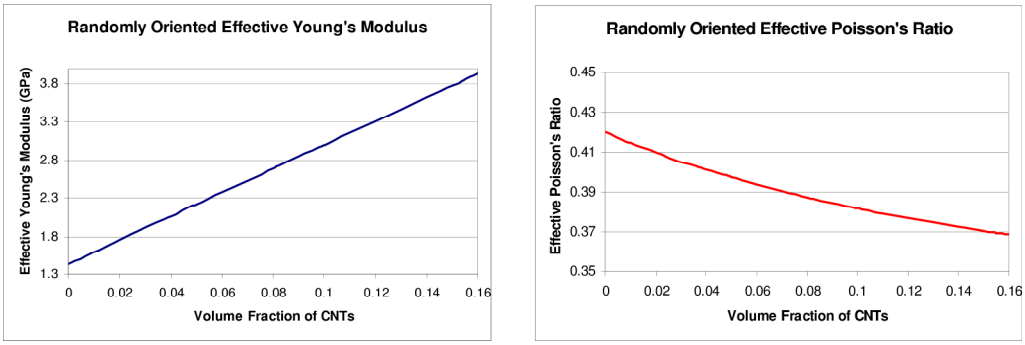

(a) (b)

Figure 6. Effective elastic properties for randomly oriented MD-equivalent continuum CNT representations obtained from Eq. (17) and used for Regions II and III of Figure 1(b) corresponding to the CNT volume faction of Figure 4. (a) Effective Young's modulus; (b) Effective Poisson's ratio.

C. Composite Cylinders Solution for Effective Lamina Properties

With the material properties of Regions II and III identified, the multi-layer composite cylinders method can be applied to determine the effective properties of the carbon fiber lamina. The effects of the sprayed CNTs on the effective lamina properties are studied in five cases below. The first two are single interphase cases, and the remaining three are multiple interphase cases. Detailed descriptions of each case and discussions on the resulting effective properties are provided below.

1. Single Interphase Solutions

Two single interphase cases, that is a composite cylinder assemblage of $N = 3$, are considered in an effort to demonstrate the different effects of Regions II and III. In the first case, the effects of having the carbon fiber in the lamina treated with a small region with a relatively high volume fraction of CNTs are investigated. This case is representative of having Region I, Region II, and Region IV only. In the second case, the effects of having the carbon fiber in the lamina treated with a larger region of CNTs, but with a variable volume fraction of CNTs are is investigated. However, in this case, which is representative of having Region I, Region III, and Region IV only, the properties for Region III are obtained from the properties of the random orientation of effective CNTs at the CNT volume fraction corresponding to the average volume fraction of Region III in Figure 4 (i.e. 4.86%). The material property and geometry data for both cases are summarized in Table 2. It should be noted that the epoxy elastic constants provided for Region IV in Table 2 were obtained from MD-equivalent continuum simulations similar to those done on the molecular RVE in obtaining the effective CNT-epoxy properties; the only difference being the lack of a CNT in the molecular RVE. Typical values for storage moduli of the neat cured epoxy are 2-3 GPa at 250-300 K.[26]

In Figure 7(a), the effect of the single interphase regions in Cases 1 and 2 on the effective axial Young's modulus (E_{11}) of the lamina are compared to the axial Young's modulus results for a carbon fiber lamina with no CNTs (i.e., a composite cylinder assemblage of $N = 2$ where the two phases are Region I and Region IV). From Figure 7(a) it is observed that the effect of the interphase region on the effective axial modulus is negligible. For the no CNT case, the axial modulus is known to be well approximated by the rule of mixtures. The axial Young's modulus for Cases 1 and 2 are similarly well approximated by a three-phase rule of mixtures, however, given the large differences between the fiber and matrix properties, and that the interphase regions are of the same order as the matrix properties, it is difficult to observe any difference between the no CNTs and single interphase cases. In fact, at carbon fiber volume fractions typically found in lamina, e.g., 60% carbon fiber, the percent difference in axial Young's modulus between Case 1 and the no CNT case is 0.0017%. For Case 2, the percent difference is 0.041%. Although not shown here, the effective Poisson's ratio of the lamina is also marginally effected by the interphase regions in Cases 1 and 2. Unlike the axial modulus, the Poisson's ratio consists of both axial and transverse strain components resulting in

Table 2. The Young's modulus and Poisson's ratio of each phase used for two single interphase composite cylinder solutions for CNT-sprayed carbon fiber lamina. The first case is indicative of a small region of a relatively high concentration of CNTs near the carbon fiber. The second case is indicative of a larger lower CNT concentration region representing the average concentration of Region III CNT volume fraction decay of Figure 4.

	Region	Radial Distance μm	Young's Modulus GPa	Poisson's Ratio
Case 1	Region I	0 - 5.0	230.00	0.3000
	Region II	5.0 - 5.004	3.8608	0.3696
	Region IV	> 5.004	1.4400	0.4200
Case 2	Region I	0 - 5.0	230.00	0.300
	Region III	5.0 - 5.3	2.2039	0.4003
	Region IV	> 5.3	1.4400	0.4200

slightly higher percent differences for Cases 1 and 2 relative to the no CNT case, e.g., 0.015% and 0.47%, respectively, at 60% carbon fiber volume fraction.

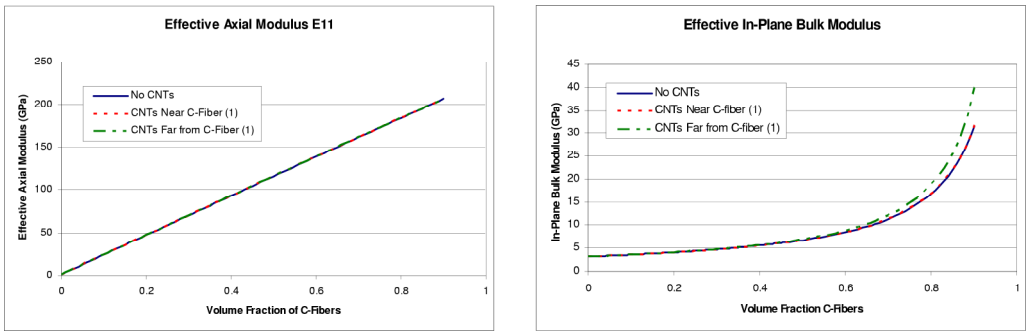

(a) (b)

Figure 7. Effective Axial Young's modulus (E_{11}) (a) and plane strain bulk modulus (κ_{23}) (b) of CNT-sprayed carbon fiber lamina. The label `No CNTs` refers to a composite cylinders assemblage for the Lamina RVE consisting of just Regions I and IV. The labels `CNTs Near C-Fiber` and `CNTs Far from C-Fiber` refer single interphase cases where the single interphase corresponds to Region II and Region III, respectively, with the Region III interphase value taken from an average of the CNT volume fraction decay in Figure 4. The number in parenthesis denotes number interphase regions.

The effective plane strain bulk modulus (κ_{23}) results for Cases 1 and 2 are compared to the no CNT case in Figure 7(b). It is observed that, despite having a higher volume fraction of CNTs in the single interphase region of Case 1, the small thickness of the interphase renders the contribution of the CNTs to the effective plane strain bulk modulus to be negligible (0.11% difference relative to the no CNT case). In contrast, the low CNT volume fraction but large thickness of the interphase region in Case 2 produces observable differences relative to the no CNT case, particularly at high carbon fiber volume fractions. At 60% carbon fiber volume fraction, the percent difference in plane strain bulk modulus for Case 2 relative to the no CNT case is 4.32% and becomes as large as 11.5% at 80% carbon fiber volume fraction. Reasons for the differences between Cases 1 and 2 can be explained in terms of the total lamina CNT volume fraction. The high CNT volume fraction, small interphase thickness of Case 1 results in a total lamina CNT volume fraction of 0.015% at 60% carbon fiber volume fraction.[a] In contrast, the low CNT volume fraction but large thickness of the interphase in Case 2 results in a lamina CNT volume fraction of 0.36% at 60% carbon fiber volume fraction. Though not shown here, the remaining effective lamina properties, G_{12}, G_{23}, and E_{22}, show very similar

[a]Note that the properties and thicknesses of the single interphase regions remain fixed as carbon fiber volume fraction varies. Increasing the carbon fiber volume fraction reduces the epoxy (Region IV) volume fraction by making r_{IV} smaller until it equals the interphase radius. As such, at higher carbon fiber volume fractions, the interphase lamina volume fraction is increased and therefore, so to is the lamina CNT volume fraction.

trends to the plane strain bulk modulus results provided in Figure 7(b). The only difference between these properties and the plane strain bulk modulus being in the magnitude of percent difference relative to the no CNT case which remains at less than 0.3% for Case 1 and is on the order of 7-8% for Case 2 at 60% carbon fiber volume fraction. As such, for the multiple interphase results which follow, only the plane strain bulk modulus will be provided.

2. *Multiple Interphase Solutions*

Table 3. The Young's modulus and Poisson's ratio of each phase used for three multiple interphase composite cylinder solutions for CNT-sprayed carbon fiber lamina. These cases are indicative of approximations of the CNT concentration region of Regions II and III CNT volume fraction decay of Figure 4.

	Region	Radial Distance μm	Young's Modulus GPa	Poisson's Ratio
2-Interphase	Region I	0 - 5.0	230.00	0.3000
	Region II	5.0 - 5.004	3.8608	0.3696
	Region III	5.004 - 5.304	2.2039	0.4003
	Region IV	$>$ 5.304	1.4400	0.4200
3-Interphase	Region I	0 - 5.0	230.00	0.3000
	Region II	5.0 - 5.004	3.8608	0.3696
	Region III.a	5.004 - 5.154	2.7286	0.3880
	Region III.b	5.154 - 5.304	1.6654	0.4128
	Region IV	$>$ 5.304	1.4400	0.4200
4-Interphase	Region I	0 - 5.0	230.00	0.3000
	Region II	5.0 - 5.004	3.8608	0.3696
	Region III.a	5.004 - 5.104	3.0036	0.3826
	Region III.b	5.104 - 5.204	2.0096	0.4030
	Region III.c	5.204 - 5.304	1.5700	0.4157
	Region IV	$>$ 5.304	1.4400	0.4200

Such large differences between Cases 1 and 2 indicate a need to accurately represent the interphase region in determining the effective lamina properties. As such, more accurate representations of the graded interphase region of CNT treated carbon fibers are also investigated through the use of multiple interphase regions. In these cases, all four regions are considered, i.e., Region I, Region II, Region III, and Region IV. The properties for Region II are obtained as previously discussed for Case 1 above. The graded interphase of Region III is represented using increasing numbers or piecewise continuous subregions. The subregion properties are obtained by taking the average Young's modulus and Poisson's ratio over the subregion thickness from the mapping of the effective properties of randomly oriented CNT-epoxy RVE into the CNT volume fraction distribution of Figure 4. The material property and geometry data for each multiple interphase case are summarized in Table 3, with the 4-Interphase Case distribution in Young's modulus shown graphically in Figure 8 and compared with the exponential decay of Eqn. (18). These three multiple interphase

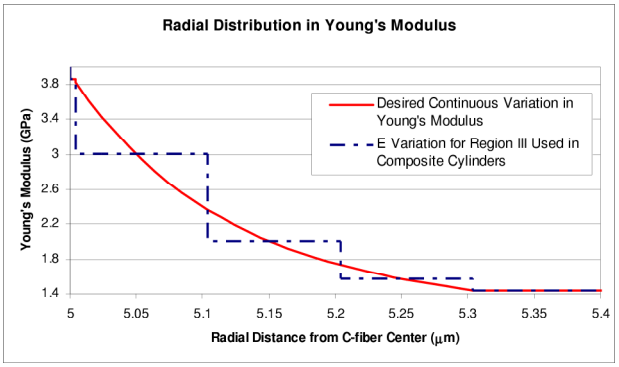

Figure 8. Radial distribution in Young's modulus in Regions II and III obtained from the correlation between the desired CNT volume fraction distribution given in Figure 4 and the random orientation Young's modulus results of Figure 6(a). Region III is approximated by three piecewise continuous subregions which, with Region II, results in a composite cylinder assemblage of $N = 6$.

cases are represented by composite cylinder assemblages of $N = 4, 5$, and 6. The 2-Interphase case represents a combination of the two single interphase cases previously discussed. The 3-Interphase and 4-Interphase cases are intended to demonstrate increasingly accurate representations of the graded interphase of Region III.

Effective plane strain bulk modulus results at high carbon fiber volume fractions (greater than 80%) are provided for all cases in Figure 9. The results in Figure 9 show that the no CNT case brackets the other cases from below while the 2-Interphase case brackets the results from above. The order of the resulting plane strain bulk moduli from the bottom up is No CNTs, Case 1, 4-Interphase, 3-Interphase, Case 2, and 2-Interphase, which at 80% carbon fiber volume fraction amounts to percent differences relative to the No CNT case of 0%, 0.28%, 9.85%, 10.19%, 11.49% and 11.85%, respectively. It is of interest to point out that the order of increasing total lamina CNT volume fraction does not exactly correspond to the order of increasing plane strain bulk modulus. The total lamina CNT volume fractions are 0%, 0.020%, 0.47%, 0.49%, 0.48% and 0.50% for the No CNTs, Case 1, 4-Interphase, 3-Interphase, Case 2, and 2-Interphase cases, respectively. The 3-Interphase case actually has a higher total lamina CNT volume fraction than Case 2 which has the higher plane strain bulk modulus of the two. This indicates the importance of the distribution of the CNTs around the carbon fiber. In Case 2 there is a uniform distribution of the CNTs in the interphase region, but in the 3-Interphase the distribution of CNTs into three separate subregions results in an average Young's modulus for the Region III interphase as a whole of 2.197 GPa which is slightly less than the Case 2 value of 2.2039 GPa.

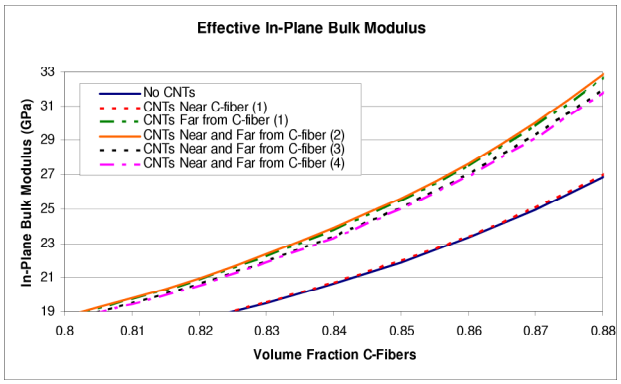

Figure 9. Effective plane strain bulk modulus (κ_{23}) of CNT-sprayed carbon fiber lamina of varying interphase representation. Results are shown only for the high carbon fiber volume fractions for clarity. The labels `NoCNTs`, `CNTs Near C-Fiber`, and `CNTs Far from C-Fiber` have been identified in Figure 7(b). The new labels `CNTs Near and Far from C-Fiber` denote Lamina RVE representations including both Regions II and III, with the number in parenthesis denoting the total number of interphase regions. The order of the curves in the figure from bottom to top is: `No CNTs`, `CNTs Near C-fiber (1)`, `CNTs Near and Far from C-fiber (4)`, `CNTs Near and Far from C-fiber (3)`, `CNTs Far from C-fiber (1)`, `CNTs Near and Far from C-fiber (2)`.

Also of note in Figure 9, as the number of interphase subregions is increased, the difference between successive increases decreases. For example, the difference between the 2-Interphase case and the 3-Interphase case relative to the no CNT case is 1.66% at 80% carbon fiber volume fraction. At the same carbon fiber volume fraction, the difference between the 3-Interphase case and the 4-Interphase case is 0.34%. This demonstrates that there is a converging effect of adding increasing number of interphases which improves the accuracy with which the graded interphase region is modeled. As such, the comparison between the most accurate case, the 4-Interphase case, and the No CNT case is provided in Figure 10 to clearly demonstrate the effectiveness of adding even a small amount of CNTs on the lamina properties of carbon fiber lamina.

IV. Conclusion

A multi-scale method has been applied to assess the effective properties of a CNT coated carbon fiber lamina. The method makes use of the molecular dynamics, equivalent continuum, and micromechanics modeling approaches. Molecular dynamics simulations in conjunction with the equivalent continuum method have been used to obtain effective properties for a molecular RVE consisting of CNTs in epoxy. The effective CNT-epoxy properties are then randomized using the Mori-Tanaka method. Finally, a multi-layer composite cylinders approach has been applied to determine the effective properties of the carbon fiber lamina using an RVE consisting of up to four regions, two of which are interphase regions between the carbon fiber and the epoxy matrix consisting of randomly oriented CNTs in epoxy. The CNT volume fraction within these interphase regions has been taken to be variable resulting in a graded interphase region which is modeled using the multi-layer composite cylinders method using increasing numbers of piecewise continuous subregions.

Effective lamina properties for various carbon fiber volume fractions were obtained, and it was found that the axial Young's modulus and Poisson's ratio were only moderately affected by the presence of the CNT graded interphase region at all volume fractions. In contrast, the transverse Young's modulus, plane strain bulk modulus, and the axial and transverse shear moduli were found to be very sensitive to the inclusion of the graded interphase region, especially at the high carbon fiber volume fractions typically found in composite lamina. For a lamina with 60% carbon fiber volume fraction, the results indicate that the transverse lamina properties may be enhanced by as much as 8%. This projected impact is better put into perspective by considering the total composite volume fraction of CNTs which for this increase in transverse properties is only 0.36% CNTs. Thus it is observed that a very small volume fraction of CNTs (0.36%) applied to the matrix surrounding carbon fibers in a lamina can have a measurable impact (8%) on the effective elastic properties associated with the direction transverse to the carbon fiber axis (E_{22}, κ_{23}, G_{23} and G_{12}).

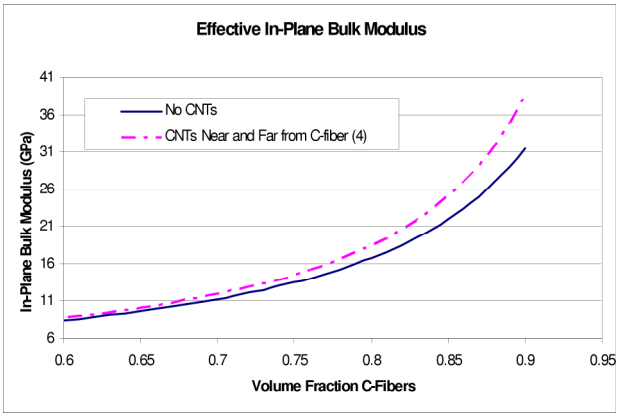

Figure 10. Effective plane strain bulk modulus (κ_{23}) of 4-Interphase representation of a CNT-sprayed carbon fiber lamina. Results are shown only for the common carbon fiber volume fractions in a given lamina.

Acknowledgments

The authors thank J.C. Riddick, J. Zhu, E. Barrera, P. Thakre, A. Awasthi, and J. Ratcliffe for their many helpful discussions. In addition, the authors would like to acknowledge the use of the NASA Ames Supercomputing Center and System X at Virginia Polytechnic Institute and State University upon which the molecular dynamics simulations were performed.

Finally, the authors also graciously acknowledge the support provided by Sandia National Laboratories, a multiprogram laboratory operated by Sandia Corporation, a Lockheed Martin Company, for the U.S. Department of Energy under Contract DE-AC04-94AL85000, and in addition, the support provided by the Texas Institute for Intelligent Bio-Nano Materials and Structures for Aerospace Vehicles, funded by NASA Cooperative Agreement No. NCC-1-02038.

References

[1]Schadler, L., Giannaris, S. C., and Ajayan, P. M., "Load transfer in carbon nanotube epoxy composites," *Applied Physics Letters*, Vol. 73, No. 26, 1998, pp. 3842–3844.

[2]Zhu, J., Kim, J., Peng, H., Margrave, J., Khabashesku, V., and Barrera, E., "Improving the dispersion and integration of single-walled carbon nanotubes in epoxy composites through functionalization," *Nano Letters*, Vol. 3, No. 8, 2003, pp. 1107–1113.

[3]Zhu, J., Peng, H., Rodriguez-Macias, F., Margrave, J., Khabashesku, V., Imam, A., Lozano, K., and Barrera, E., "Reinforcing epoxy polymer composites through covalent integration of functionalized nanotubes," *Advanced Functional Materials*, Vol. 14, No. 7, 2004, pp. 643–648.

[4]Li, C. and Chou, T.-W., "Multiscale modeling of carbon nanotube reinforced polymer composites," *Journal of Nanoscience and Nanotechnology*, Vol. 3, No. 6, 2003, pp. 1–8.

[5]Frankland, S., Odegard, G., Herzog, M., Gates, T., and Fay, C., "Constitutive modeling of cross-linked nanotube materials with variable stiffness tethers," *ASC/ASTM-D30 Joint 19th Annual Technical Conference*, ASC, Atlanta, GA, October 17-20 2004.

[6]Gates, T., Odegard, G., Nemeth, M., and Frankland, S., "Predicting the Influence of Nano-scale Material Structure on the In-plane Buckling of Orthotropic Plates," *45th AIAA/ASME/ASCE/AHS/ASC Structures, Stuctural Dynamics, and Materials Conference*, AIAA-2004-1607, 2004.

[7]Odegard, G., Frankland, S., and Gates, T., "Effect of Nanotube Functionalization on the Elastic Properties of Polyethylene Nanotube Composites," *AIAA Journal*, Vol. 43, No. 8, August 2005, pp. 1828–1835, AIAA-9468-376.

[8]Gates, T., Odegard, G., Frankland, S., and Clancy, T., *Composite Science and Technology*, Vol. 65, 2005, pp. 2416.

[9]Gao, X.-L. and Li, K., "A shear-lag model for carbon nanotube-reinforced polymer composites," *International Journal of Solids and Structures*, Vol. 42, 2005, pp. 1649–1667.

[10]Gou, J., Liang, Z., Zhang, C., and Wang, B., *Composites Part B*, Vol. 36, 2005, pp. 524–533.

[11]Clancy, T. and Gates, T., "Mechanical Properties of Nanostructured Materials Determined through Molecular Modeling Techniques," *46th AIAA/ASME/ASCE/AHS/ASC Structures, Stuctural Dynamics, and Materials Conference*, AIAA-2005-1852, 2005.

[12]Hashin, Z. and Rosen, B., "The elastic moduli of fiber-reinforced materials," *Journal of Applied Mechanics*, Vol. 31, 1964, pp. 223–232.

[13]Christensen, R. and Lo, K., "Solutions for effective shear properties in three phase sphere and cylinder models," *Journal of the Mechanics and Physics of Solids*, Vol. 27, 1979, pp. 315–330.

[14]Carman, G., Averill, R., Reifsnider, K., and Reddy, J., "Optimization of fiber coatings to minimize stress concentrations in composite materials," *Journal of Composite Materials*, Vol. 27, No. 6, 1993, pp. 589–612.

[15]Herve, E. and Zaoui, A., "Elastic behaviour of multiply coated fibre-reinforced composites," *International Journal of Engineering Science*, Vol. 33, No. 10, 1995, pp. 1419–1433.

[16]Seidel, G. and Lagoudas, D., "Micromechanical analysis of the effective elastic properties of carbon nanotube reinforced composites," *Mechanics of Materials*, In Press.

[17]Mori, T. and Tanaka, K., "Average stress in matrix and average elastic energy of materials with misfitting inclusions," *Acta Metallurgica*, Vol. 21, 1973, pp. 571–574.

[18]Benveniste, Y., "A new approach to the application of Mori-Tanaka's theory in composite materials," *Mechanics of Materials*, Vol. 6, 1987, pp. 147–157.

[19]Eshelby, J., "The determination of the elastic field of an ellipsoidal inclusion, and related problems," *Proceedings of the Royal Society of London*, Vol. 241, No. 1226, 1957, pp. 376–396.

[20]Odegard, G., Gates, T., Wise, K., Park, C., and Siochi, E., "Constitutive modeling of nanotube-reinforced polymer composites," *Composites Science and Technology*, Vol. 63, 2003, pp. 1671–1687.

[21]Cornell, W., Cieplak, P., Bayly, C., Gould, I., Merz, K., Ferguson, D., Spellmeyer, D., Fox, T., Caldwell, J., and Kollman, P., *Journal of the American Chemical Society*, Vol. 117, 1995, pp. 5179.

[22]Plimpton, S., *Journal of Computational Physics*, Vol. 117, 1995, pp. 1.

[23]Smith, W. and Forester, T., "DL-POLY," Tech. rep., Daresbury, Nr. Warrington, England: The Council for the Central Laboratory of the Research Councils, 1996.

[24]Group, H. P. C. C., "NWChem, A Computational Chemistry Package for Parallel Computers, Version 4.5," Tech. rep., Pacific Northwest National Laboratory, Richland, WA, 2003.

[25]Saito, R., Dresselhaus, G., and Dresselhaus, M., *Physical Properties of Carbon Nanotubes*, Imperial College Press, 1998.

[26]Kaeble, D., Moacanin, J., and Gupta, A., "Physical and Mechanical Properties of Cured Resins," *Epoxy Resins: Chemistry and Technology*, Vol. 2nd, 1988, pp. 603–651.